2012 IEEE/RSJ International Conference on
Intelligent Robots and Systems
October 7-12, 2012. Vilamoura, Algarve, Portugal

Non-ideal Behaviors of Magnetically Driven Screws in Soft Tissue

Arthur W. Mahoney, Nathan D. Nelson, Erin M. Parsons, and Jake J. Abbott

Abstract— **This paper considers the requirements for stable control of simple devices that consist of a permanent magnet rigidly attached to a screw operating in soft tissue. Placing these devices in a rotating magnetic field causes the device's permanent magnet to rotate synchronously with the applied field, making the attached screw generate forward propulsion. Although there has been significant research in the area of magnetic screws, this paper describes magnetic phenomena that have not been addressed in prior work, yet will be critical in the design of future steering and control strategies for medical applications. Using a time-averaged model of magnetic torque, we analyze the magnetic torque present when intentionally steering the screw or due to naturally occurring disturbances in the screw's heading. We predict and experimentally demonstrate the existence of magnetic torques that simultaneously act to stabilize and destabilize magnetic screws operating in tissue. We find that there exists an applied field rotation speed, above which screws may become unstable, and we find that the interaction between the stabilizing and destabilizing magnetic torques may cause potentially undesired but predictable behavior while steering.**

I. Introduction

Untethered micro- and mesoscale actuated devices (e.g., microrobots) have become an active area of research in the field of minimally invasive medicine due to their potential for locomotion and manipulation in hard-to-reach areas of the human body [1]. Many applications of interest will require such devices to locomote through soft tissue. These may include radioactive seed positioning for prostate brachytherapy, positioning an untethered device within the brain for hyperthermia treatments, and navigating through the vitreous humor of the eye to perform therapy of the retina such as targeted drug delivery.

One form of untethered device that is showing promise for medical applications are those actuated using forces and torques produced by magnetic fields. The helical microswimmer, which consists of a rigid helix attached to a magnetic element designed to mimic the motion of bacterial flagella, is one such device [2]–[4]. When placed in a rotating magnetic field, a torque is applied to the device through the magnetic head, which causes the attached helix to rotate and produce fluidic propulsion. Helical microswimmers operate well in the low-Reynolds-number regime where viscous drag dominates inertia [5]. Because the helix of the microswimmer does not displace the medium around the magnetic head, helical microswimmers are not well suited for moving through soft tissue. Instead, similar devices that consist of a magnetic element attached to a solid screw, rather than a helix, have been proposed for use in tissue [6]–[11].

In [6], the authors introduce a device of 11.5 mm in length consisting of a 7.5 mm-long diametrically magnetized permanent magnet attached to a 4.0 mm-long brass wood screw. While operating their devices in agar gel to simulate tissue, the authors show that their device's forward velocity is linearly related to the rotation frequency of the applied field, and they demonstrate that their device can be used in real tissue by driving it through a 25 mm-thick sample of bovine tissue. In [7], the authors demonstrate that by pitching the rotation axis of the rotating applied field out of alignment with the principal axis of the screw, the devices can be made to steer toward a desired direction in agar gel. In their experiments, they find that the smallest turning radius can be obtained with their shortest device when the applied field rotates at 0.1 Hz and the rotation axis of the applied field is kept pitched away from the principal axis of their screw by 60° toward the direction of the desired turn. The authors show that the average magnetic torque causing their device to turn is maximized in this configuration, and that applying torque in this manner generates turns of highest curvature. Other research has explored various screw-tip cutting mechanisms [8], trailing a wire [9], local hyperthermia treatment using inductive heating [10], and using screw devices as pH sensors [11].

This paper continues on the work of [6] and [7] toward stable open-loop control of untethered screw devices in soft tissue. In this study, we numerically analyze the time-averaged magnetic torque that causes the screw to pitch in the direction of the applied field's axis of rotation, which is present when intentionally steering the screw or due to naturally occurring disturbances in the screw's heading. We show that not only is there a stabilizing magnetic torque that causes the screw to realign with the rotation axis of the applied field as desired, but there also always exists a competing undesired destabilizing magnetic torque that simultaneously causes the screw to turn perpendicular to the desired direction of alignment. We demonstrate that there exists a rotation speed of the applied field above which the destabilizing torque will always be greater in magnitude than the stabilizing torque. This can cause the screw to become unstable and diverge away from the desired trajectory. This phenomenon is not documented in prior literature and must be taken into account when designed future steering and control strategies for medical applications.

This material is based upon work supported by the National Science Foundation under Grant Nos. 0952718 and 0654414.

A. W. Mahoney is with the School of Computing, and N. D. Nelson, E. M. Parsons, and J. J. Abbott are with the Department of Mechanical Engineering, University of Utah, UT 84112, USA.
email: art.mahoney@utah.edu

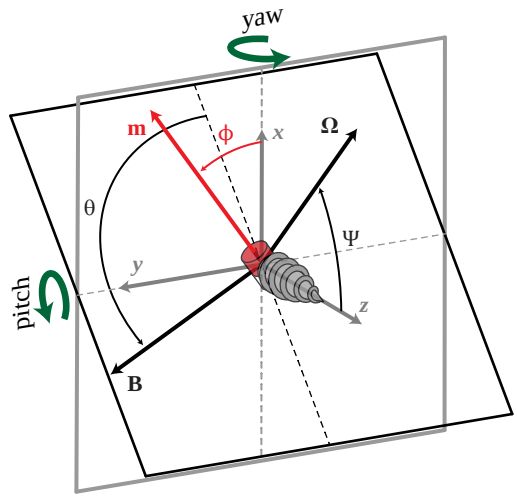

Fig. 1. The principal axis of the untethered screw device is constrained to lie parallel to the $\mathbf{z}$ device axis making the dipole moment of the screw $\mathbf{m}$ lie in the $\mathbf{x}$-$\mathbf{y}$ screw plane. The applied magnetic field (magnetic flux density) $\mathbf{B}$ rotates around and is perpendicular to the rotation axis $\boldsymbol{\Omega}$. The screw is steered in space by pitching $\boldsymbol{\Omega}$ away from the screw's principal axis by the angle ψ toward the desired direction of steering.

II. Modeling Magnetic Control

Let the applied magnetic field $\mathbf{B}$ (magnetic flux density) rotate with angular velocity $\boldsymbol{\Omega}$, whose direction and magnitude define the applied field's axis of rotation and speed, and where $\mathbf{B}$ is perpendicular to $\boldsymbol{\Omega}$. Define a device coordinate frame with axes $\{\mathbf{x},\mathbf{y},\mathbf{z}\}$ as shown in Fig. 1, where the $\mathbf{z}$ axis is parallel to the screw's principal axis, the $\mathbf{x}$ axis lies in the plane spanned by the $\mathbf{z}$ axis and $\boldsymbol{\Omega}$, and the $\mathbf{y}$ axis lies in the direction of $\mathbf{z} \times \mathbf{x}$. This breaks down when $\mathbf{z}$ is parallel to $\boldsymbol{\Omega}$, however, this paper is concerned with the case when $\mathbf{z}$ is not parallel to $\boldsymbol{\Omega}$. For simplicity, we assume that the screw's principal axis lies parallel to the $\mathbf{z}$ device axis. We define ψ to measure the angle between $\mathbf{z}$ and $\boldsymbol{\Omega}$, which we refer to as the "pitch angle."

The instantaneous magnetic torque $\boldsymbol{\tau}$ produced on a dipole moment $\mathbf{m}$ (i.e., the small permanent magnet attached to the screw) by $\mathbf{B}$ at the location of $\mathbf{m}$ causes $\mathbf{m}$ to align with $\mathbf{B}$ and is expressed by $\boldsymbol{\tau} = \mathbf{m} \times \mathbf{B}$. We have chosen to parameterize $\mathbf{m}$ and $\mathbf{B}$ with the angles, ϕ and θ, respectively, which results in the representations

$$\mathbf{B} = |\mathbf{B}| \begin{bmatrix} \cos\psi\cos\theta \\ \sin\theta \\ -\sin\psi\cos\theta \end{bmatrix} \tag{1}$$

$$\mathbf{m} = |\mathbf{m}| \begin{bmatrix} \cos\phi \\ \sin\phi \\ 0 \end{bmatrix} \tag{2}$$

and the resulting magnetic torque $\boldsymbol{\tau}$ is given by

$$\boldsymbol{\tau} = |\mathbf{m}||\mathbf{B}| \begin{bmatrix} \sin\psi\cos\theta\sin\phi \\ -\sin\psi\cos\theta\cos\phi \\ \sin\theta\cos\phi - \cos\psi\cos\theta\sin\phi \end{bmatrix} \tag{3}$$

We denote the components of $\boldsymbol{\tau}$ that lie parallel to the $\mathbf{x}$ and $\mathbf{y}$ device axis to be the destabilizing $\boldsymbol{\tau}_x$ and stabilizing $\boldsymbol{\tau}_y$ torques, respectively. The component of $\boldsymbol{\tau}$ in the device $\mathbf{z}$ direction, $\boldsymbol{\tau}_z$, causes the screw to roll and is referred to as the propulsion torque. When $\boldsymbol{\Omega}$ is aligned with the principal axis of the screw (i.e., $\psi = 0°$), the magnetic torque is purely composed of the propulsion torque, and the components representing the stabilizing and destabilizing magnetic torques have zero magnitude. The result is a linear trajectory in the direction of the screw's principal axis.

The screw is steered through space by pitching the rotation axis $\boldsymbol{\Omega}$ of the applied field in the direction of the desired turn. Without loss of generality, $\boldsymbol{\Omega}$ is assumed to be rotated about the $\mathbf{y}$ device axis. When $\boldsymbol{\Omega}$ is not aligned with the principal axis of the screw, the stabilizing $\boldsymbol{\tau}_y$ and destabilizing $\boldsymbol{\tau}_x$ magnetic torques cause the screw to align with and deviate from $\boldsymbol{\Omega}$, respectively. In Newtonian fluids, the screw responds by aligning its principal axis with $\boldsymbol{\Omega}$ over time [2]. In viscoelastic environments such as soft tissue, however, the stabilizing and destabilizing magnetic torques introduce complex steering behavior.

Rather than model the complex behavior, we have chosen to simplify analysis by examining the average stabilizing and destabilizing torques over one revolution of the applied field, the assumption being that the tendency of the screw to change its heading in the stabilizing or destabilizing directions during one applied field revolution will be related to the averaged stabilizing or destabilizing torques during the same field revolution, while operating in tissue.

The model used to average the stabilizing and destabilizing torque is derived by constraining the screw as if it were placed within a lumen such that the stabilizing and destabilizing torques have no effect on the screw's heading and the screw only rotates about its principal axis (i.e., ϕ is time-varying but ψ is constant). The model is simplified in this way because, in practice, the screw rotates much faster about its principal axis than it changes its heading when operating in tissue. When averaging over one revolution of the applied field, even with the presence of the stabilizing and destabilizing torques, the actual change in heading due to these torques is small and will not significantly alter the analysis of the averaged torques themselves.

The dominating motion during one applied field revolution will be the screw's rotation around its principal axis. This rotation is modeled with the assumption that any inertial effects are dominated by linear drag caused by friction between the screw and the tissue, making the inertial torque negligible. The net torque acting upon the screw along its principal axis consists of the magnetic torque generated by the applied field and a linear damping torque. This assumption is often made when analyzing helical swimmers in low-Reynolds-regime fluids where fluidic drag dominates inertia [5]. Aside from torque, forces that act on the screw in tissue include the force due to gravity and any forces acting on the screw due to the mechanics of the tissue itself. Due to the force acting on the screw from the tissue, the screw typically does not sink under the force of gravity as it would in Newtonian fluids [3] and we assume its effect is negligible. The full effect of the forces caused by tissue mechanics remains to be studied.

The linear damping torque about the screw's principal axis is modeled with the coefficient c and is $|\boldsymbol{\tau}_f| = c\dot{\phi}$, where $\dot{\phi}$ is the angular velocity of the screw about the same axis. The magnetic torque applied about the screw's principal axis is $\boldsymbol{\tau}_z$, whose magnitude is found in (3). Since the net torque is zero, the differential equation governing the rotational dynamics of the screw about its principal axis, for some constant pitch angle ψ and constant field rotation speed $|\boldsymbol{\Omega}|$, can be found as

$$\dot{\phi} = \frac{|\mathbf{m}||\mathbf{B}|}{c}\big(\sin\theta(t)\cos\phi(t) - \cos\psi\cos\theta(t)\sin\phi(t)\big) \quad (4)$$

which can be solved numerically given initial conditions $\phi(0)$ and $\theta(0)$, since $\theta(t) = |\boldsymbol{\Omega}|t$ is known for all t.

The solution $\phi(t)$ of (4) describes the screw's rotational response to the rotating field for the given pitch angle ψ and field rotation speed $|\boldsymbol{\Omega}|$. There exists a field rotation speed $|\boldsymbol{\Omega}|$, above which the screw's rotation cannot remain synchronized with the rotating field. This speed, known as the "step-out" speed, is a function of the linear damping term c, the field magnitude $|\mathbf{B}|$, the screw dipole moment $|\mathbf{m}|$, the pitch angle ψ, and is given by $|\mathbf{m}||\mathbf{B}|\cos(\psi)/c$. When $|\boldsymbol{\Omega}|$ is larger than the step-out frequency, the screw tends to behave chaotically and control is limited. When $|\boldsymbol{\Omega}|$ is less than step-out, the screw remains synchronized with the rotating field, although the magnetic torque $\boldsymbol{\tau}$ tends to oscillate.

After solving (4) numerically to produce $\phi(t)$ for a given pitch angle ψ and field rotation speed $|\boldsymbol{\Omega}|$, the magnitude of the torque about the $\mathbf{y}$ axis and the $\mathbf{x}$ axis averaged over one turn of the applied field is produced by integrating the $\mathbf{x}$ and $\mathbf{y}$ components of (3) using the numerical solutions for $\phi(t)$ and $\theta(t)$ to obtain $\phi(\theta)$, which is used in the integrations

$$\bar{\boldsymbol{\tau}}_x = \frac{|\mathbf{m}||\mathbf{B}|}{2\pi}\sin\psi\int_{2\pi k}^{2\pi(k+1)}\cos\theta\sin\big(\phi(\theta)\big)d\theta \quad (5)$$

$$\bar{\boldsymbol{\tau}}_y = -\frac{|\mathbf{m}||\mathbf{B}|}{2\pi}\sin\psi\int_{2\pi k}^{2\pi(k+1)}\cos\theta\cos\big(\phi(\theta)\big)d\theta \quad (6)$$

where $k \in \mathbb{Z}^+$ is selected to reject the screw's transient response due to the initial conditions when solving (4). Although we have observed the initial transient response to be insignificant after two rotations of the applied field, we chose $k = 9$ as a conservative lower limit of integration with initial conditions $\phi(0) = 0°$ and $\theta(0) = 90°$. Averaging the magnetic torque after the transient response simplifies analyses by removing fluctuation caused by the oscillation in $\boldsymbol{\tau}$. Neglecting the transient response, the values obtained for $\bar{\boldsymbol{\tau}}_x$ and $\bar{\boldsymbol{\tau}}_y$ only change with the pitch angle ψ and field rotation speed $|\boldsymbol{\Omega}|$ used to obtain the solution of (4).

We find that $\bar{\boldsymbol{\tau}}_x$ and $\bar{\boldsymbol{\tau}}_y$ can be normalized by scaling them by the maximum possible total magnetic torque $|\mathbf{m}||\mathbf{B}|$, and they can be enumerated over the pitch angle ψ and the normalized field rotation speed, which is defined as the ratio of $|\boldsymbol{\Omega}|$ to the screw's step-out speed when $\psi = 0°$. Fig. 2(a) and Fig. 2(b) show non-dimensional contour plots of normalized $\bar{\boldsymbol{\tau}}_x$ and $\bar{\boldsymbol{\tau}}_y$ with $\psi \in [0°, 90°)$. Because the screw's step-out speed varies with ψ, and we are interested in the screw's behavior when the screw is synchronized with

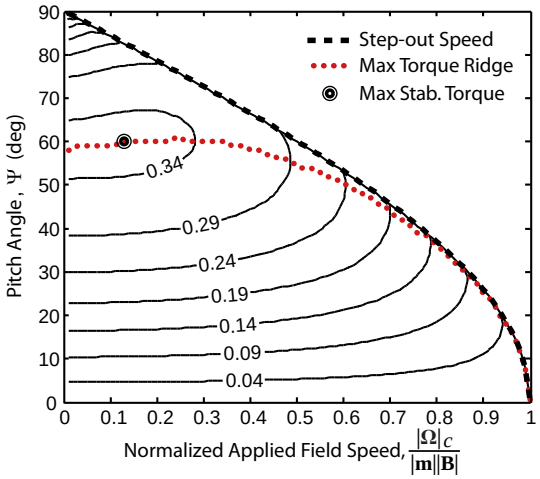

(a) Average scaled stabilizing torque, $\bar{\boldsymbol{\tau}}_y/|\mathbf{m}||\mathbf{B}|$. The maximum stabilizing torque occurs at a normalized rotation speed of 0.13 and pitch angle 60.0°. The curve "Max Torque Ridge" describes the pitch angle necessary to maximize stabilizing torque for each normalized applied field rotation speed.

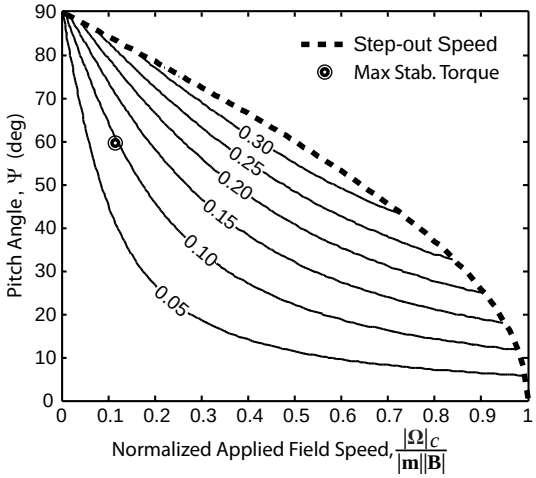

(b) Average scaled destabilizing torque, $\bar{\boldsymbol{\tau}}_x/|\mathbf{m}||\mathbf{B}|$.

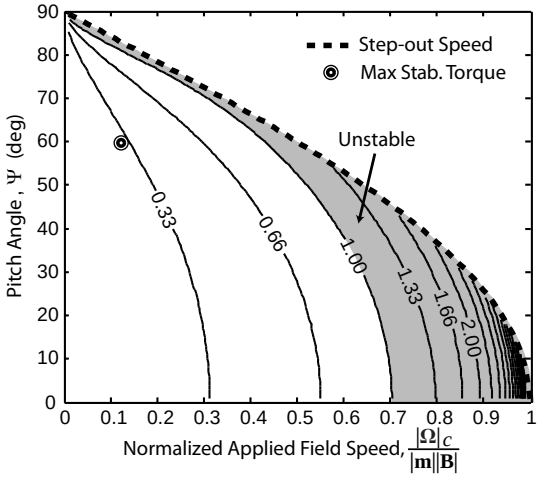

(c) Ratio of the average destabilizing torque to average stabilizing torque, $\bar{\boldsymbol{\tau}}_x/\bar{\boldsymbol{\tau}}_y$. The region where the screw becomes unstable is labeled and shaded.

Fig. 2. The average stabilizing torque (a), average destabilizing torque (b), and the ratio between them (c), as a function of the pitch angle and normalized applied field rotation speed. The point where the maximum stabilizing torque occurs is shown in all three contour plots for reference.

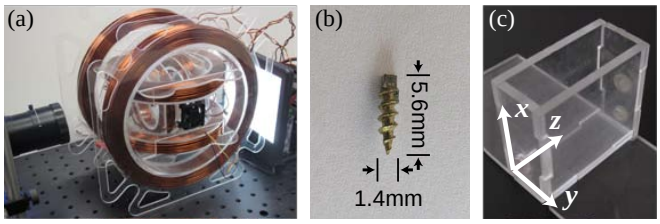

Fig. 3. The Helmholtz coils (a), the untethered screw device (b), and the container (c) used for experiments presented in this paper. The screw device is 5.6 mm long and 1.4 mm in diameter and consists of a 1 mm cube permanent magnet rigidly attached to brass screw with 0.87 mm pitch. The static world coordinate frame used in experiments is shown in (c).

the rotating field, the normalized field rotation speed was ranged so as not to exceed step-out for each value of ψ. The step-out speed is shown as a bold, dashed line. When $\mathbf{\Omega}$ is pitched down (i.e., $\psi < 0°$), the results of Fig. 2(a) and Fig. 2(b) change sign but Fig. 2(c) is unchanged.

Fig. 2(a) shows the average stabilizing torque that causes the screw to turn toward $\mathbf{\Omega}$ increases with ψ up to the curve labeled "Max Torque Ridge" for any field rotation speed with the global scaled maximum of 0.35 occurring at normalized rotation speed of 0.13 and pitch angle of $60.0°$ (which corresponds to the same result found by [7]). As the average stabilizing torque increases, Fig. 2(b) shows that the average destabilizing torque tends to increase as well, and can become larger than the stabilizing torque. The region of Fig. 2(c) where the ratio between the average destabilizing and stabilizing torques is larger than one corresponds to configurations where the average destabilizing torque is larger than the average stabilizing torque. When operating in this region, the magnetic torque will produce more rotation of the screw away from than toward $\mathbf{\Omega}$. If the screw's heading is deviated from $\mathbf{\Omega}$, due to naturally occurring disturbances, then the screw may become unstable when the average destabilizing torque is large. Operating the screw so that the average stabilizing torque is larger than the average destabilizing torque will enable the screw to reject disturbances, realigning faster when the stabilizing torque dominates the destabilizing torque.

From Fig. 2(b), the averaged destabilizing torque is only zero when $\psi = 0°$ or $|\mathbf{\Omega}| = 0$. This means that while steering the screw by increasing or decreasing ψ, there will always be a destabilizing torque present that causes the screw to yaw in the direction perpendicular to the desired turn. When the desired turn direction is up in Fig. 1 (i.e., $\psi > 0°$), the destabilizing torque will cause the screw to yaw around the positive $\mathbf{x}$ device axis according to the right-hand rule. When the desired turn direction is down in Fig. 1 (i.e., $\psi < 0°$), the destabilizing torque creates yaw around the negative $\mathbf{x}$ device axis. Although the screw will always have the tendency to yaw, its effect can be reduced by operating in regions of Fig. 2(b) where the average destabilizing torque is small (i.e. at small angles of ψ and/or at slow speeds).

III. Experimental Results

The experimental setup used to generate controlled magnetic fields consists of three nested sets of Helmholtz coils (described in detail in [3] and shown in Fig. 3(a)) arranged orthogonally such that the magnetic field in the center of the coils can be assigned arbitrarily, with each Helmholtz pair corresponding to one basis direction of the magnetic field. Each set of Helmholtz coils generates a magnetic field that is approximately uniform in the center of the workspace, with a maximum field strength of $10\,\text{mT}$. Computer vision for screw tracking was performed using a Basler A602FC camera fitted with a Computar MLH-10X macro zoom lens with the image plane parallel to the $\mathbf{x}$-$\mathbf{z}$ plane of a static world coordinate frame, depicted in Fig. 3(c).

Similarly to [6] and [7], agar gel was used to simulate soft tissue for our experiments. Agar gel is commonly used in research as an inexpensive and semi-transparent tissue phantom. For example, agar gel has been used to simulate the vitreous humor of the eye [12], brain tissue [13], and human breast tissue [14]. The agar gel used herein consisted of 0.5 wt. % culinary agar to unfiltered water, which we found to handle well for our initial experiments. For a comparison, it has been found that 0.6 wt. % agar closely models properties of human brain tissue [13]. Our agar gel was cut into blocks, fitting a $45\,\text{mm}\times16\,\text{mm}\times38\,\text{mm}$ acrylic container, and positioned in the common center of the Helmholtz coils. The screw used in this study is $5.6\,\text{mm}$ long and $1.4\,\text{mm}$ in diameter and consists of a $1\,\text{mm}$ cube Grade-N50 permanent magnet rigidly attached to a brass wood screw with $0.87\,\text{mm}$ pitch. During experimentation, the step-out frequency of the screw at $\psi = 0°$ ranged from $7.3\,\text{Hz}$ to $8.0\,\text{Hz}$ and the field strength $|\mathbf{B}|$ was set to $10.0\,\text{mT}$.

The screw's ability to reject disturbances in orientation is demonstrated in the results presented in Fig. 4, which shows several screw trajectories as viewed from the imaging system with $\mathbf{\Omega}$ aligned with the world's $\mathbf{z}$ axis throughout the duration of each run. Four typical trajectories when operating at normalized applied field rotation speeds of 0.20 and 0.85 are shown on the left side of Fig. 4(a) and Fig. 4(b), respectively, along with the points where each trajectory exits the agar sample plotted on the right. At normalized speed 0.20, the average stabilizing torque is sufficient to overcome the average destabilizing torque and return the orientation of the screw to $\mathbf{\Omega}$ resulting in a tight clustering of exit points near the opposite position of the entry point. With normalized speed of 0.85, the average destabilizing torque overcomes the stabilizing torque and perpetually increases the magnitude of naturally occurring disturbances resulting in unstable behavior and large variation in the position of the exit points as shown. It is important to note, however, that the screw only naturally rejects disturbances in heading, not position. The position of the screw may drift off the desired trajectory without feedback control.

We demonstrate the screw's tendency to yaw while steering by pitching $\mathbf{\Omega}$ an angle of ψ measured from the screw's principal axis as seen from the vision system. As the screw

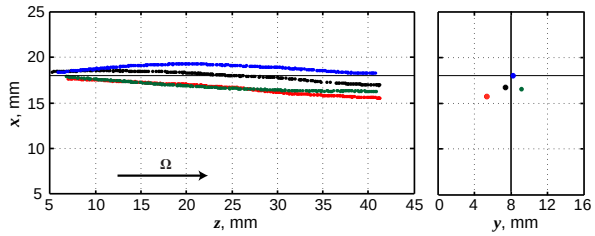

(a) Normalized applied field speed 0.20

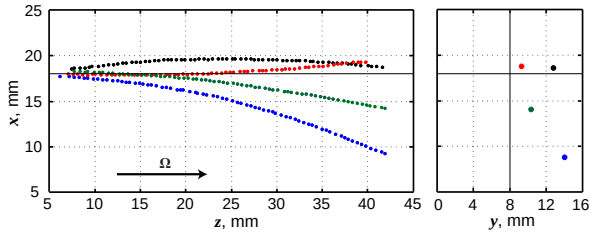

(b) Normalized applied field speed 0.85

Fig. 4. Trajectories of the screw at two applied field rotation speeds in agar gel (0.5 wt. %) with $\mathbf{\Omega}$ parallel to the $\mathbf{z}$ world axis. The exit points of each trajectory are shown on the right side of the figure. Each trajectory is obtained using the computer vision system. Each exit point is measured by hand.

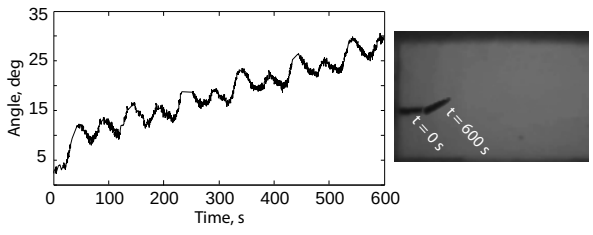

(a) Normalized applied field speed 0.001 and $\psi = 10.0°$

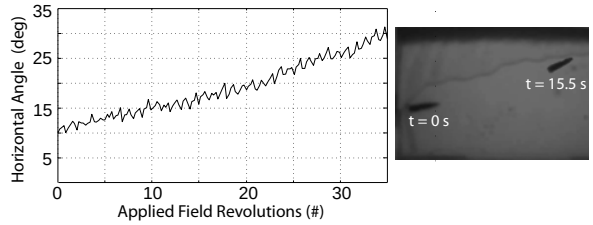

(b) Normalized applied field speed 0.3 and $\psi = 10.0°$

Fig. 6. Angle of the screw's principal axis measured from horizontal as a function of the number of applied field revolutions while rotating at a normalized rotation speed of 0.001 (a) and 0.3 (b). The right side shows images of the screw in the agar at the beginning and end of the experiment.

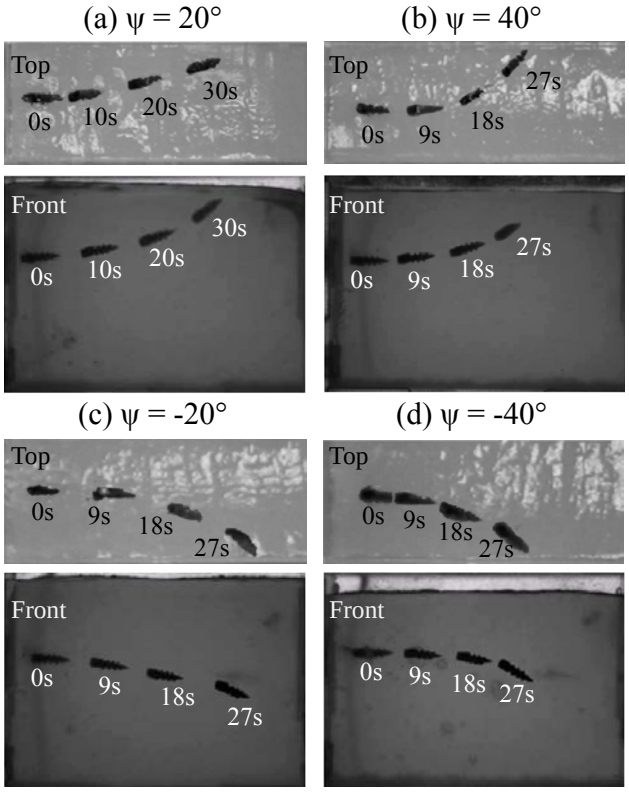

Fig. 5. Front and top views of screw trajectories demonstrating the screw's tendency to yaw while turning. The angle between the screw's principal axis and $\mathbf{\Omega}$ (as viewed from the $\mathbf{x}$-$\mathbf{z}$ world plane) is maintained at $\psi = \pm 20°$ and $\pm 40°$. The field is rotated at a normalized applied field rotation speed of 0.20 in all four cases.

turns, $\mathbf{\Omega}$ was kept in the $\mathbf{x}$-$\mathbf{z}$ world plane, but manually adjusted to maintain a constant ψ using visual feedback with the assistance of guidelines drawn on realtime video of the screw presented to the user. Fig. 5 shows a front view (in the $\mathbf{x}$-$\mathbf{z}$ world plane) and a top view (in the $\mathbf{y}$-$\mathbf{z}$ world plane, taken with a Canon PowerShot G10) of the resulting trajectories with $\psi = 20°$ and $40°$ in Figs. 5(a) and 5(b), and $\psi = -20°$ and $-40°$ in Figs. 5(c) and 5(d), respectively. In all four cases, the applied field is rotated at a normalized rotation speed of 0.20 and each trajectory stops when the screw either collides with the container or exits the top of the agar sample. When $\psi > 0°$, Fig. 2 predicts that the stabilizing torque will cause the screw to turn in the direction of $\mathbf{\Omega}$ but the destabilizing torque will cause the screw to rotate about the $\mathbf{x}$ axis of the device frame. In the world frame, the screw will tend to simultaneously turn about the $\mathbf{y}$ world axis and the $\mathbf{z}$ world axis as shown in Figs. 5(a) and 5(b). When $\psi < 0°$, the screw will tend to simultaneously turn about the $-\mathbf{y}$ world axis and the $-\mathbf{z}$ world axis as shown in Figs. 5(c) and 5(d). This tendency to yaw will need to be taken into account while navigating untethered screws devices.

In Sec. II, we applied the assumption that the screw's principal axis is constrained during one complete rotation of the applied field. This tends to be a valid assumption when driving the screw through tissue because the heading of the principal axis typically does not change significantly over one revolution of the applied field. This assumption breaks down when rotating the applied field very slowly. At slow rotation speeds, the instantaneous magnetic torque (3) causes the screw's heading to vary significantly throughout one cycle. This is demonstrated in Fig. 6, which shows the measured heading of the screw (obtained using the computer vision system) as a function of time when driving the screw with a normalized applied field rotation speed of 0.001 and 0.3, with the pitch angle ψ the same in both cases. When rotating the applied field slowly, the screw's heading tends to oscillate at a magnitude of 7° throughout one

applied field revolution, whereas the screw's heading tends to oscillate at a magnitude of 1° when rotating the applied field rapidly. Without any explicit understanding of the screw-tissue interaction, the drop in magnitude may indicate that the oscillations of the screw exceed the inherent bandwidth of the tissue. If the oscillation of the screw is undesired (e.g., due to potential tissue damage), then the screw should be driven at faster rotation speeds, which may come at the cost of increasing the undesired yaw while steering.

IV. Discussion

Various screw geometries have been proposed for driving through soft tissue. In [6], the authors propose a similar device to that used in our experiments, where a permanent magnet is rigidly attached to a single screw; in [7] and [8], the authors control a screw-like device consisting of a helical thread wrapped around a cylindrical permanent magnet (diametrically magnetized); and in [11], the authors propose a device consisting of screws rigidly attached to both ends of a cylindrical permanent magnet. The results presented in Sec. II are purely an analysis of the interaction between the screw's dipole moment and the applied magnetic field, therefore, it applies to screws of any geometry. Because the magnetic torque applied to the screw is a pure torque (i.e., not an immediate result of an applied force), its affect on the screw (as a free body) is invariant to where it is applied on the device itself. As a result, the screw used herein would exhibit the same behavior if the cube magnet were positioned in the middle of the screw as it does with the magnet positioned at the rear. We do expect, however, that the screw's length and the density of the tissue will influence the magnitude of the behavior demonstrated herein.

The screw used herein is $5.6\,\text{mm}$ long. It is likely that the screw will need to be scaled down for many medical applications. We do not yet have a good understanding of screw-tissue interaction. However, we can approximate the role of friction as the screw is scaled if we model the screw as if it were a cylinder and if we assume that the friction between the tissue and the screw is proportional to the surface area. Applying these assumptions, the surface area of the screw is $A = 2\pi dl$, where d and l are the screw's diameter and length. If d and l are scaled by a factor s, then the surface area becomes $A = 2\pi dls^2$ and thus scales with s^2. If we scale the dimensions of the permanent magnet rigidly attached to the screw by the same factor s, then the magnet's volume scales with s^3. The magnitude of the screw's dipole moment $\mathbf{m}$ is proportional to the magnet's volume causing $\mathbf{m}$, and subsequently the applied magnetic torque $\boldsymbol{\tau}$ (given by (3)), to also scale with s^3. This implies that as the screw is scaled down, the surface friction decreases at a slower rate than the magnetic torque and the applied magnetic field magnitude $|\mathbf{B}|$ may need to increase to generate effectively the same behavior presented herein. Fully understanding how the screw will scale to smaller sizes will require the screw-tissue interaction to be better understood. This will be the subject of future work.

V. Conclusion

In this study, we have analyzed the stabilizing and destabilizing magnetic torques present when intentionally steering an untethered screw device or due to naturally occurring disturbances in the screw's heading. We have shown theoretically and experimentally that there exists an applied field rotation speed, above which untethered screws devices will become unstable. We have also demonstrated that complex interaction between the stabilizing and destabilizing magnetic torques can cause a screw device to turn away from desired directions of steering in a predictable way. These phenomena are not reported in prior literature and they must be taken into account when designing future steering and closed-loop control strategies for medical applications.

Acknowledgment

The authors wish to thank Jeremy Greer and Dr. Eberhard Bamberg for fabricating the screw pictured in Fig. 3.

References

[1] B. J. Nelson, I. K. Kaliakatsos, and J. J. Abbott, "Microrobots for minimally invasive medicine," *Annu. Rev. of Biomed. Eng.*, vol. 12, pp. 55–85, 2010.

[2] L. Zhang, J. J. Abbott, L. X. Dong, B. E. Kratochvil, D. Bell, and B. J. Nelson, "Artificial bacterial flagella: Fabrication and magnetic control," *Appl. Phys. Lett.*, vol. 94, no. 064107, 2009.

[3] A. W. Mahoney, J. C. Sarrazin, E. Bamberg, and J. J. Abbott, "Velocity control with gravity compensation for magnetic helical microswimmers," *Advanced Robotics*, vol. 25, no. 8, pp. 1007–1028, 2011.

[4] K. E. Peyer, A. W. Mahoney, L. Zhang, J. J. Abbott, and B. J. Nelson, "Bacteria-inspired microrobots," in *Microbiorobotics: Biologically Inspired Microscale Robotic Systems*, 1st ed., M. J. Kim et al., Ed. Oxford: Elsevier, 2012, pp. 156–199.

[5] J. J. Abbott, K. E. Peyer, M. Cosentino Lagomarsino, L. Zhang, L. X. Dong, I. K. Kaliakatsos, and B. J. Nelson, "How should microrobots swim?" *Int. J. Robotics Research*, vol. 28, no. 11–12, pp. 1434–1447, 2009.

[6] K. Ishiyama, M. Sendoh, A. Yamazaki, and K. I. Arai, "Swimming micro-machine driven by magnetic torque," *Sensors and Actuators A*, vol. 91, no. 1–2, pp. 141–144, 2001.

[7] M. Sendoh, K. Ishiyama, and K. I. Arai, "Direction and individual control of magnetic micromachine," *IEEE Trans. Magn.*, vol. 38, no. 5, pp. 3356–3358, 2002.

[8] M. Sendoh, A. Yamazaki, A. Chiba, M. Soma, K. Ishiyama, and K.I. Arai, "Spiral type magnetic micro actuators for medical applications," in *Proc. Int. Symp. Micro-Nanomechatronics and Human Science*, 2004, pp. 319–324.

[9] K. Kikuchi, A. Yamazaki, M. Sendoh, K. Ishiyama, and K. Arai, "Fabrication of a spiral type magnetic micromachine for trailing a wire." *IEEE Trans. Magn.*, vol. 39, no. 10, pp. 4012–4014, 2005.

[10] F. Sato, M. Jojo, H. Matsuki, T. Sato, and M. Sendoh, "The operation of a magnetic micromachine for hyperthermia and its exothermic characteristic," *IEEE Trans. Magn.*, vol. 38, no. 4, pp. 3362–3364, 2002.

[11] B. H. McNaughton, J. N. Anker, and R. Kopelman, "Magnetic microdrill as a modulated fluorescent pH sensor," *J. Magn. Magn. Mater.*, vol. 293, no. 1, pp. 696–701, 2005.

[12] M. P. Kummer, J. J. Abbott, S. Dinser, and B. J. Nelson, "Artificial vitreous humor for in vitro experiments," in *Proc. of IEEE Int. Conf. Engineering in Medicine and Biology Society*, 2007, pp. pp.6406–6409.

[13] Z. J. Chen, G. T. Gillies, W. C. Broaddus, S. S. Prabhu, H. Fillmore, R. M. Mitchell, F. D. Corwin, and P. P. Fatouros, "A realistic brain tissue phantom for intraparenchymal infusion studies," *J. Neurosurg.*, vol. 101, no. 2, pp. 314–322, 2004.

[14] K. Zell, J. I. Sperl, M. W. Vogel, R. Niessner, and C. Haisch, "Acoustical properties of selected tissue phantom materials for ultrasound imaging," *Phys. Med. Biol.*, vol. 52, no. 20, pp. 475–484, 2007.